Pure Appl. Geophys. 175 (2018), 1669–1681

https://doi.org/10.1007/s00024-017-1719-3

Pure and Applied Geophysics

Parallel Observations with Three Superconducting Gravity Sensors During 2014–2015 at Metsähovi Geodetic Research Station, Finland

Heikki Virtanen[1] and Arttu Raja-Halli[1]

Abstract—The new dual-sphere superconducting gravimeter (SG) OSG-073 was installed at Metsähovi Geodetic Fundamental Station in Southern Finland in February 2014. Its two gravity sensors (N6 and N7) are side by side, not one on top of the other as in other earlier dual-sensor installations. The old SG T020 has been recording continuously since 1994–2016. This instrument is situated in the same room at a distance of 3 m from the dual-sphere SG. T020 observed simultaneously for 1 year with N6 and for 15 months with N7. The gravity signals observed by N6 and N7 are very similar, except for the initial exponential drift. We have calculated the power spectral density to compare the noise level of these instruments with other low noise SGs. In this paper we present the observed differences in the gravity time series of T020 and OSG-073, induced by local hydrology. We have observed a clear 10–20 nms^{-2} difference in the seasonal gravity variations of OSG-073 and T020. We have found clear gravity differences due to transient effect of heavy precipitation. In addition, we compare the remote effect on gravity due to variations in the Baltic Sea level and total water storage in Finland to the observed gravity signal. We also present modeling results of gravity variations due to local hydrology.

Key words: Superconducting gravimeter, gravity gradiometry, hydrology.

1. Introduction

1.1. Metsähovi Geodetic Fundamental Station

Finnish Geospatial Research Institute, FGI (Formerly Finnish Geodetic Institute) operates a specially designed gravity laboratory at Metsähovi Geodetic Fundamental station (ME). The building and the gravimeter piers stand on a knoll of Precambrian granite giving it a solid foundation. The station is located in a rural area. There are no industrial plants or transport arteries in the near vicinity of the station that could cause ground vibrations. Hence, ME belongs to the group of low background noise stations among other GGP stations (Rosat and Hinderer 2011). ME is a multi-technique geodetic research station and is a part of the GGOS's (Global Geodetic Observing System) core sites, including absolute gravity (AG), permanent GNSS, Satellite Laser Ranging (SLR), DORIS beacon and geodetic VLBI (Very long Baseline Interferometry). All techniques are influenced by the same environmental loading effects as the SG. Because of its high sensitivity, the SG is an excellent tool for testing and validating the pertinent correction models. Within a distance of 100 m from the gravity laboratory there are multiple automated hydrological sensors for hydrological studies: 3 deep boreholes in the bedrock, 11 groundwater observation tubes in the sediments, 12 arrays of soil-moisture sensors and a pluviometer (Mäkinen et al. 2014; Hokkanen et al. 2006). In addition, the water equivalent of snow is measured with Campbell CS725 as well as manually. In 2015, the station was equipped with a new Vaisala weather station AWS310. Besides the fundamental sensors (pressure, temperature, humidity, wind, precipitation), two pyranometers, one for global radiation and one for ground radiation, and an ultrasonic snow depth sensor are included in the weather station. These sensors are necessary for hydrological modeling. The rain gauge is heated (to measure also precipitation as snow) and is equipped with a Tretyakov windshield. The map of local area is presented in Fig. 1. Together with the gravity data it is possible to model the gravitational effect due to changes in atmospheric mass distributions, hydrological conditions and in the Baltic Sea level.

[1] Finnish Geospatial Research Institute-FGI, National Land Survey, Geodeetinrinne 2, 02430 Masala, Finland. E-mail: heikki.virtanen@nls.fi

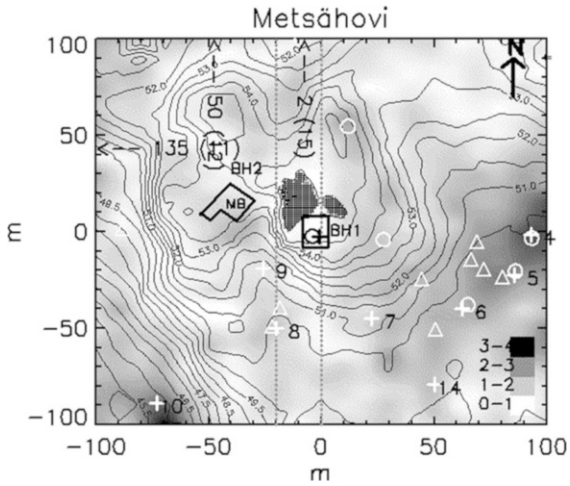

Figure 1
Map of the Metsähovi area (200 × 200 m) included in our local modeling. The isolines at 0.5-m interval show surface elevations and the gray shades show soil thickness, dark areas North of the gravity lab are bare bedrock above gravity sensors. Maximum soil thickness is 3.7 m, mean value is 0.8 m. The SG T020 is in the center, marked by a cross inside the gravity laboratory and OSG-022 marked by a circle 3 m to the West. The SG sensor is at 55.6 m elevation. MB denotes main building. Numbered crosses mark the places of the groundwater tubes in soil. Three tubes are outside the plotted area. Tube 8 used in Fig. 7 is at about (− 20, − 50 m) in local coordinates. Triangles denote arrays of soil-moisture sensors. BH1 (just E from the gravity laboratory) and BH2 are borehole wells in bedrock. A third borehole well for water use is inside the main building (NW from the gravity laboratory). Small circles denote dry access tubes. They are not used in this paper. The dotted lines are height profiles shown in Fig. 12

1.2. ME Superconducting Gravimeters

The SG of the FGI, GWR T020, has operated continuously at ME since August 1994 (Virtanen and Kääriäinen 1995, 1997). The new dual-sphere (sensor) gravimeter OSG-073 was installed in Metsähovi in February 2014 at a distance of 3 meters from SG T020 (Fig. 2). One sensor (N7) was the standard iGrav^{TM}, with a lightweight sphere (0.005 kg), which has a low drift rate. The second sensor (N6) uses a heavy 0.02 kg sphere which gives a very low noise with a much higher quality factor Q. Its novel design was unique: two gravity sensors are separate and side by side (15 cm), not one on top of the other as in most of the earlier dual-sensor installations (Goodkind 1999). Advantage of dual sensor is, e.g., correction of offsets and other instrumental errors (Hinderer et al. 2007).

There were four dual-sphere SGs operating around the world with normal lightweight sensors (0.005 kg sphere). At Black Forest Observatory, Germany (BFO), the lower sensor is a heavy (0.02 kg sphere) sensor (OSG-056L).

The noise level of these instruments and a comparison to NLNM (Peterson 1993) was estimated with a power spectral density (PSD) calculation (Fig. 3). For the PSD calculation we have used 5 days of data from days without microseism or other environmental or instrumental d levels of N7 and T020 are quite similar when compared. The sensor N6 has a very low noise, comparable to the best known gravimetric instruments in the world, such as at BFO.

We have two sets of simultaneous absolute gravity measurements with FG5X-221 at Metsähovi. In spite of the length of the SG time series (9 and 7 days), the accuracies were not very good. During the calibration measurements there were strong

Figure 2
Superconducting gravimeters at Metsähovi on November 2014. The old T020 is on the left and the new OSG-073 on the right. The distance between gravity sensors is 3.0 m. The sensor height is about 20 cm higher in T020

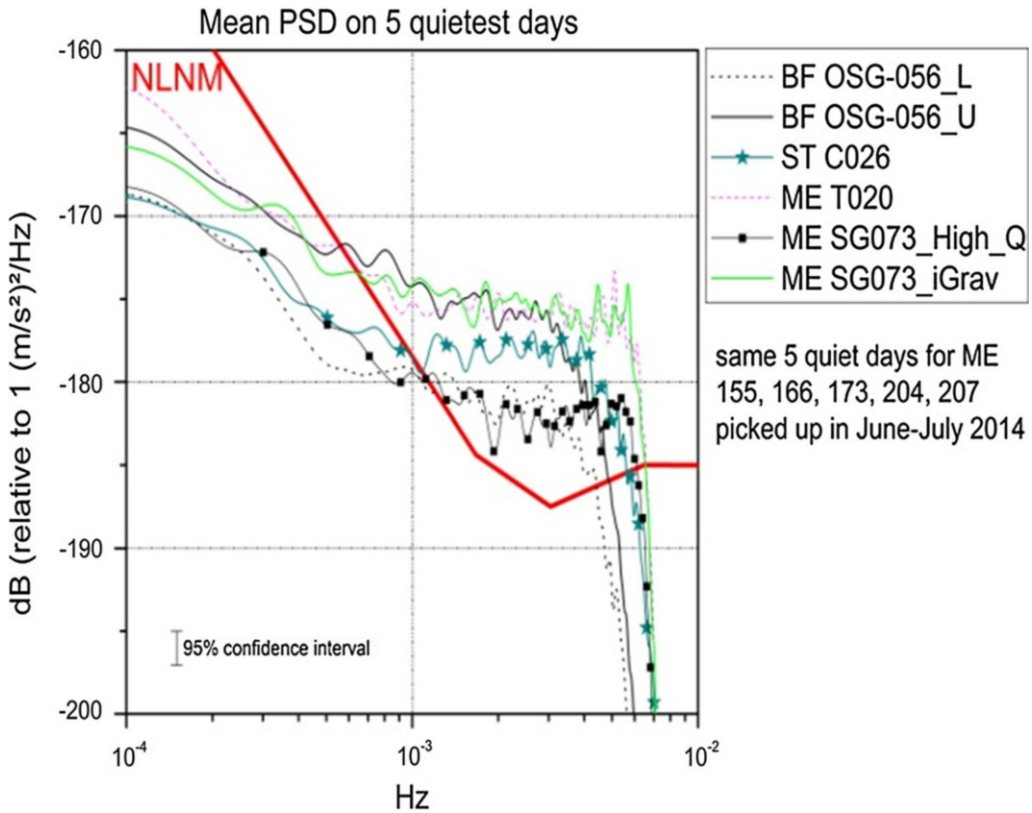

Figure 3
Noise levels for different gravity sensors (Rosat et al. 2016, Private communication). BF OSG-056_L means Black Forest Observatory (Schiltach) lower high-Q sensor, ST C026 refers to the high_Q sensor in Strasbourg, J9 station, ME SG073 High-Q is N6 and ME SG073_iGrav is N7. NLNM model is the red curve (Peterson 1993)

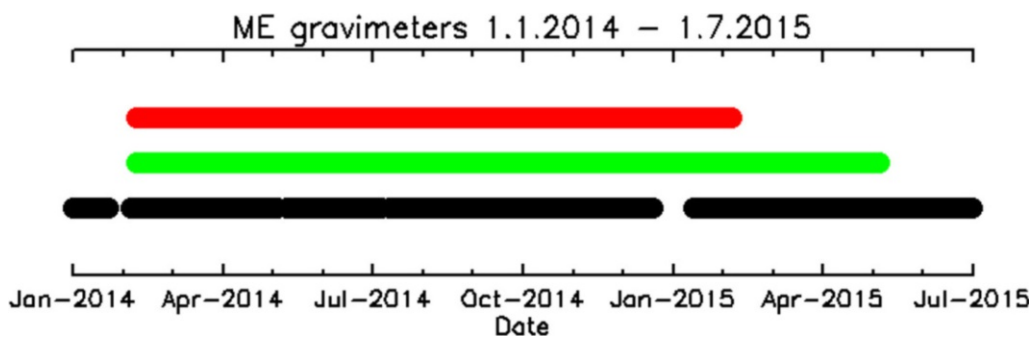

Figure 4
Parallel observations with the three gravimeters between 2014 and 2015. N6 is shown in red, N7 in green and T020 in black

microseisms, data gaps and technical problems with N6. The calculated values for the calibration factor were: N6 − 447.11 ± 0.37 and N7 − 932.47 ± 0.75 nms^2/V for N6 and N7, respectively. However, we have a very good calibration for SG T020 (Virtanen et al. 2014). We used 24 different datasets between 2003 and 2012, extending over 2–7 days with parallel FG5 measurements. The resulting calibration factor

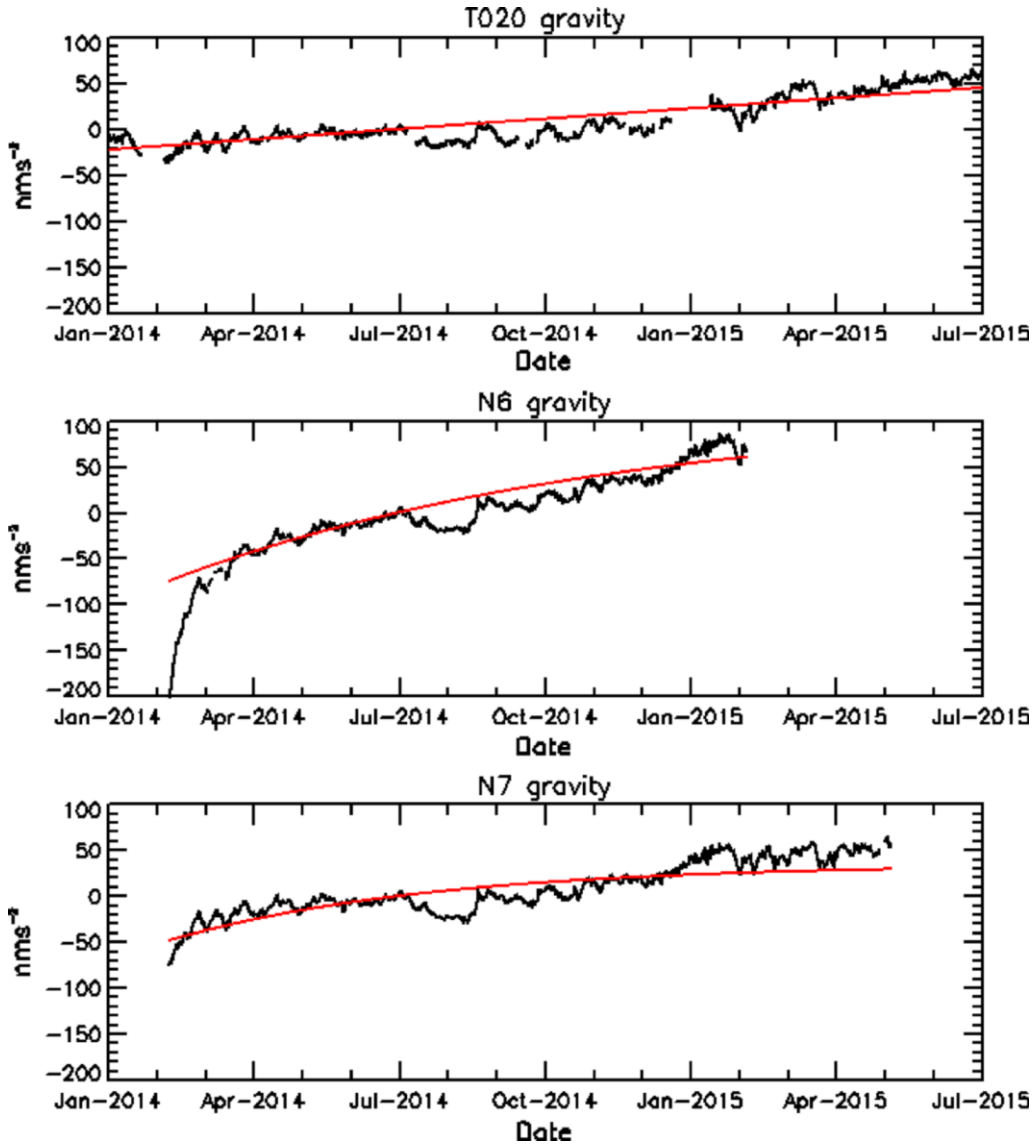

Figure 5
Gravity residuals of three sensors 1 Jan 2014–1 Jul 7 2015. Tides, atmospheric effect and pole tide were corrected. Offsets were corrected and traces of big earthquakes removed. Drift correction models for T020, N6 and N7 sensors are plotted in red lines. We have applied a linear trend for T020 sensor. Due to large non-linear drift after initialization, we have applied an exponential drift model to N6 and N7

for T020 is -1104.3 ± 1.2 nms^2/V. Hence, using T020 to calibrate sensors N6 and N7 we got calibration factors -447.53 ± 0.04 (N6) and -933.34 ± 0.08 (N7) nms^2/V. The usable length of the time series was about 164 days. We have taken into account different drift behavior of the instruments and have rejected disturbed data. Transfer functions for N6 and N7 were determined by step pulses.

The operation of T020 was finished in September 2016. The instrument has the second longest gravity data series in IGETS database, as shown in its documentation (Voigt et al. 2016). The OSG-073 was sent back to the manufacturer for improvements (GWR) in May 2015. Therefore, T020 observed simultaneously with N6 for one year and with N7 for 15 months. Observation periods for the three instruments are given in Fig. 4.

2. Data Processing

We have usable common data with T020 and N7 from Feb 2014 to 4th of May 2015, i.e., a total of 15 months. The common data set with N6 stopped on 4th of Feb 2015 due to technical problems. Some parts of T020 data were unusable due to breakage of its cooling system (Fig. 5). These problems caused an unmodeled drift to data and were handled as gaps. Original 1-s data were decimated to 1 min for cleaning and preprocessing. Cleaning process was standard (Hinderer et al. 2007, Virtanen 2006), consisting of, e.g., removal of spikes, offsets, traces of earthquakes and other disturbances. A few offsets of N6 and N7 were due to lightning detected by the Finnish Meteorological Institute. T020 had several offsets due to cooling problems, and were corrected using the OSG-073 observations. We have exploited TSOFT software and data analysis tools (Van Camp and Vauterin 2005). After cleaning the time series from disturbances we have applied an observed local tidal model (Virtanen 2006), air pressure (AP) correction with a single admittance ($-$ 3.10 nms^{-2} hPa^{-1}) and local pole tide correction, using IERS pole coordinates (https://www.iers.org).

Measured time lags for the sensors N7, T020 and N6 are correspondingly 9.5, 9.7 and 20.2 s. Time lag between N7 and T020 is very small and does not cause a significant error in the gravity signal. Instead the phase lag of N6 can cause errors in gravity up to 1.8 nms^{-2}. We have used tidal correction for N6 with a 10-s phase lag compared to T020. We have used for air pressure admittance a generic value based on several tidal analyses (Virtanen 2006).

In time domain the mean standard deviations (STD) of 1-min residual data were 0.20, 0.40, 0.50 nms^{-2}, respectively, for N6, N7 and T020.

For drift corrections and analyses shown in Table 1 we have used hourly values. Next step was the determination of drift models for the time series. We have used a linear model for the old SG T020. Due to a large non-linear drift after initialization of OSG-073, we have applied an exponential drift model by fitting the function

$$f(x_i) = c_0\, e\, c_1\, (x_i) + c_2,$$

where x_i are hourly gravity values, and c_0, c_1 and c_2 are coefficients to be determined by least-squares fitting.

Fits were applied to data after 1st of Mar 2014. For longer time series this approach is not valid, as the drift becomes nearly linear. Exponential modeling is evidently better for SGs, which are just initialized. Drift models are shown in Fig. 5. Approximate linear drifts (around Feb 2015) are for T020, N6 and N7: 4.5, 130 and 75 nms^{-2}/year. The drifts included both instrumental and geophysical parts. Geophysical part (7 nms^{-2} year^{-1}) is due to the post-glacial land uplift, which is about 2 mm/year at Metsähovi (Virtanen et al. 2014).

3. Results of Gravity Comparison Between the Three Sensors

3.1. Remote Effects on Gravity

We consider remote effects so that the gravity effect is uniform at ME, i.e., place of the gravity

Table 1

SG instrument, STD standard deviations of gravity residuals (1. col.) and regression coefficients (last col.) fitted to the remote water storage (TW) and Baltic Sea level (HSL) data

SG	TW		Baltic sea		
	STD	REG TW	REG HSL	COR	STD
T020	9.8	0.18	23.1	0.80	5.9
N6	10.8	0.23	18.2	0.86	5.5
N7	11.7	0.27	15.3	0.90	5.1

REG TW = regression coefficients for TW (nms^{-2} mm^{-1}), REG HSL = regression coefficient for HSL (nm/s^{-2} m^{-1}). Calculations are from 1st Apr–19th Dec 2014. The reduction of variance of N7 sensor is 81%

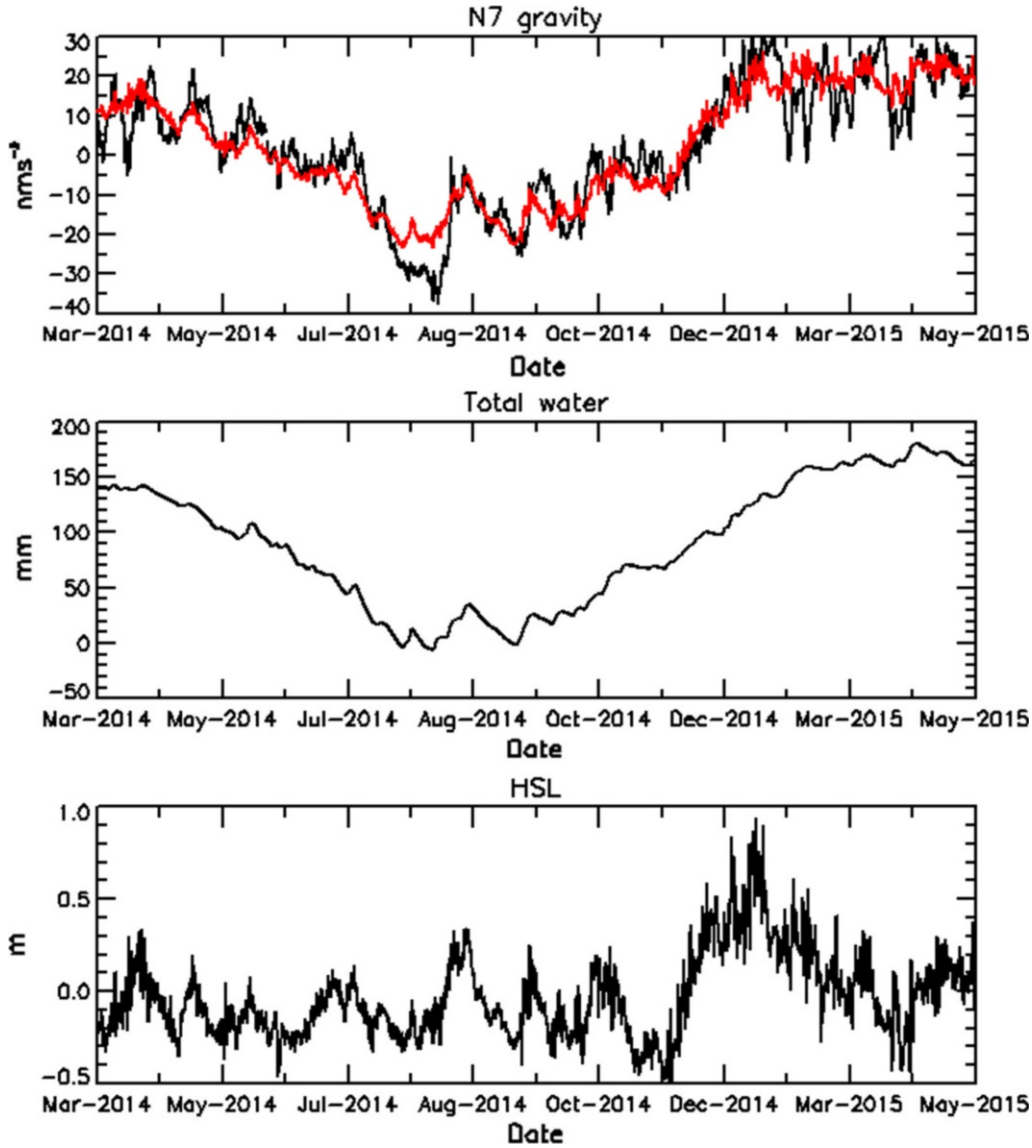

Figure 6
Top: drift-corrected N7 gravity residual (black) and fit to total water in Finland (WSFS) and HSL presented (red). Middle: total water (WSFS). Bottom: HSL (Baltic Sea level in Helsinki tide gauge) (1 Mar 2014–1 Mar 2015)

sensor at Metsähovi has no role. The drift-corrected gravity time series of N7 (1st of Mar 2014–1st of Mar 2015) is presented in Fig. 6 (top panel, black line). For comparison we have calculated STD of residuals for all three sensors (Table 1). We also calculated simultaneous linear regressions with remote water storage (TW, Fig. 6, middle panel) and Baltic Sea level changes at the Helsinki tide gauge (HSL, Fig. 6, bottom panel). TW estimates the total water storage change of Finland based on WSFS (Watershed simulation and forecast System) provided by the Finnish Environmental Institute (Vehviläinen 2007). Gravity acts as independent data and remote effects are dependent variables. Results are shown in Table 1. There are remarkable differences between the coefficients. These can be due to imperfect initial drift estimates (N6, N7) and offset corrections of T020. We got the best results for the sensor N7, for

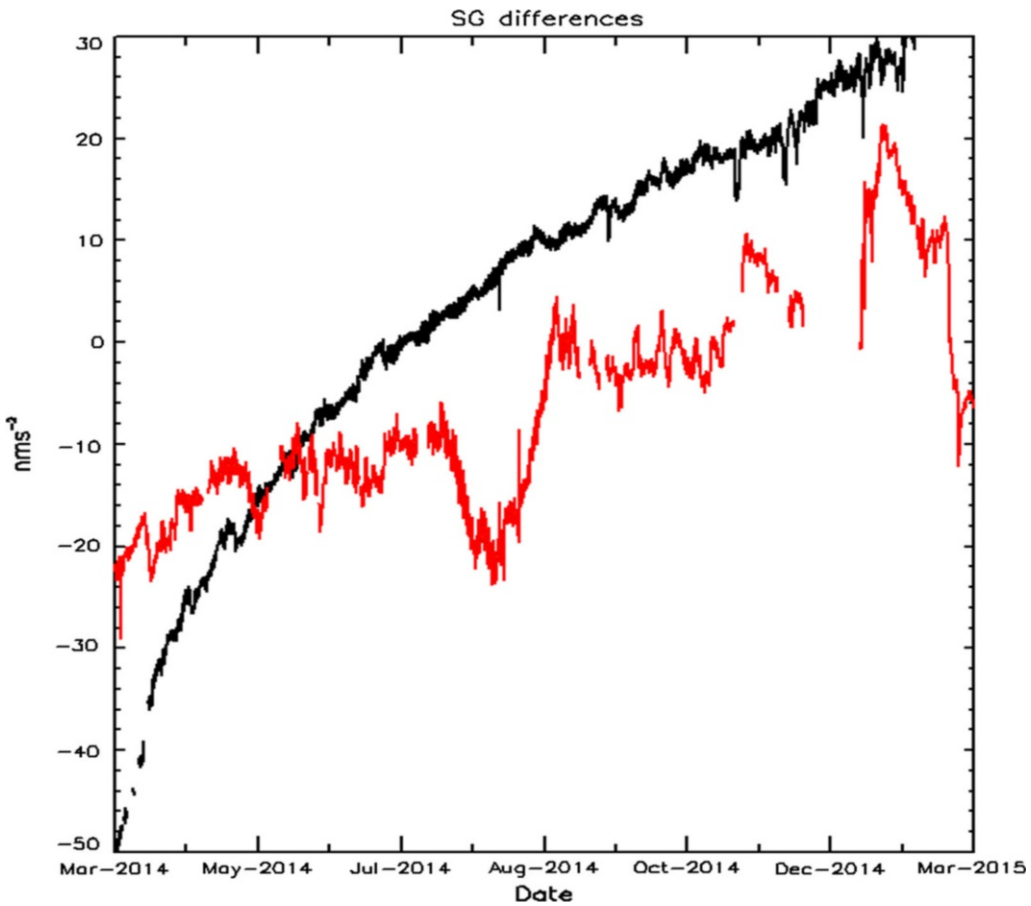

Figure 7
Difference of the gravity data series observed by N6 and N7 (black) and N7-T020 (red) from 1 Mar 2014 to 1 Mar 2015. Traces of big earthquakes and offsets were corrected, other corrections were not applied

which the variance is reduced by 81% (red color) when compared to the original time series. The fitted gravity response to TW and HSL (not residual) is shown in Fig. 6 (upper panel, red line). We have selected these environmental observations due to their well-known effect to gravity at ME (Virtanen et al. 2014).

3.2. *Local Effect on Gravity*

Local effects are mainly related due to mass changes at about 100 m distance around the gravity laboratory, where there is installed a variety of hydrological sensors (Fig. 1). The differences in the gravity observations of the three sensors are shown in Fig. 7. Gravitational effects of air pressure, tide and polar motion, TW and HSL are presumably similar to all three sensors. Hence, differences are due to instrumental drift and local mass variations, i.e., local hydrology. Discrepancies between N6 and N7 sensors are small and mainly due to the different noise levels and drift of the sensors. Larger differences between OSG-073 sensors can arise due to very close masses, e.g. visitors inside the gravity laboratory. A human body near the gravimeter can cause a different signal at sensors which are 15 cm apart. We can clearly see a long-term difference between OSG–073 and T020 sensors in Fig. 7. In Fig. 8 we present the drift-corrected gravity difference (N7-T020) together with local hydrological observations using data from the boreholes in the bedrock, soil-moisture sensors and water tubes in the soil. The locations of the

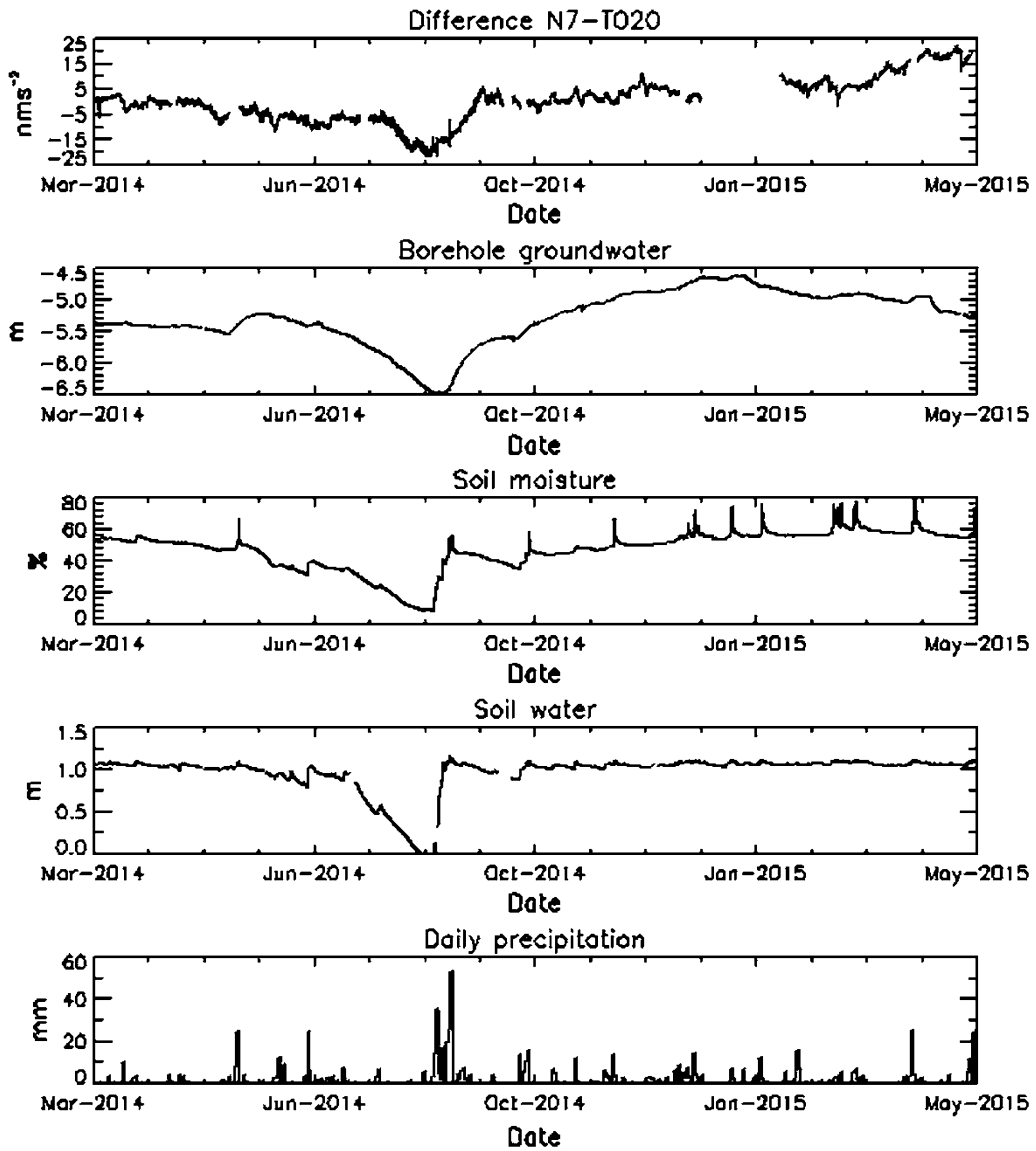

Figure 8
Top panel: gravity difference of drift-corrected N7 and T020 sensors (nms^{-2}). Second panel: groundwater in bedrock tube BH2 (m) below surface. Third panel: soil-moisture (%), sensor location is shown in ME map (Fig. 1). Fourth panel: water level in a soil ground access tube 8 m shown in ME map. Bottom panel shows daily precipitation (mm). Series are from 1 Mar 2014 to 1 May 2015

hydrological instruments are shown in Fig. 2. In addition, we get daily precipitation amount from a rain gauge, located near the gravity laboratory. All observations show similar long-term features.

A strong rain event can produce a different response of the gravity sensors. In Fig. 9 we show an example of heavy precipitation on the 20th of Aug 2014 at ME for sensors N6, N7 and T020. Daily precipitation was approximately 50 mm and the maximum intensity was 30 mm within an half an hour period. That happens very seldom at ME. Peaks caused by this event can be seen in Figs. 7 and 8.

We only found 15 days, when the gravity data of all three sensors were usable for studying the gravitational effect of precipitation. In many cases during heavy rain we had to reject data due to, e.g.,

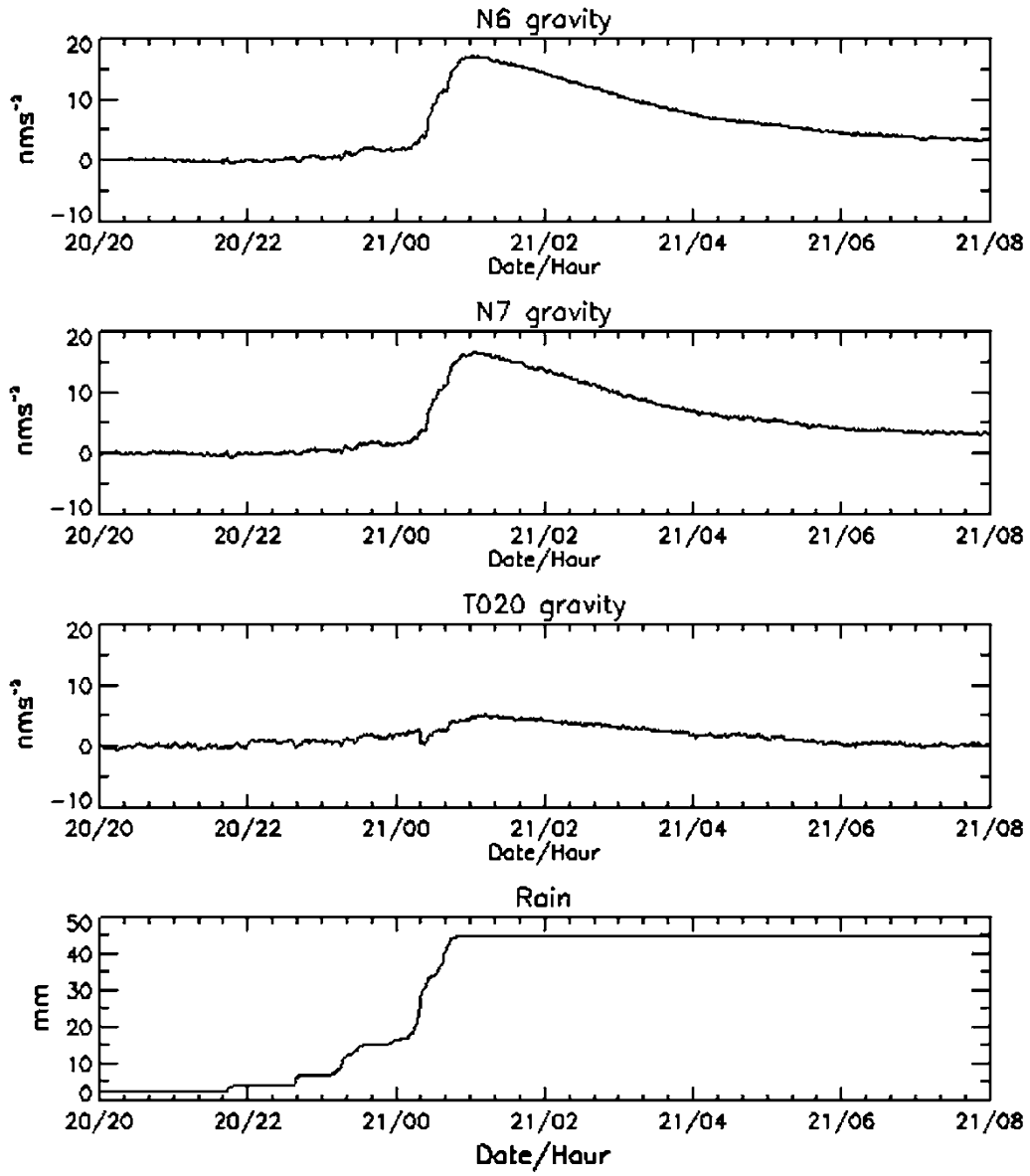

Figure 9
Gravity variations of three sensors during heavy rainfall (30 mm/0.5 h) on 20 August 2014

lightning, data gaps, saturation of the feedback of N6 or failure of the cooling system of T020. All studied rain events are presented in Table 2. The calculated gravity variation due to precipitation events are compiled in Table 2 and shown in Fig. 10. For sensor N7, we get the result 0.41 nm/s^2/mm, which is close to the Bouguer plate approximation. Time-varying gravity due to local hydrology is depending on precipitation and evaporation. Mathematical models are presented by Meurers (2007) and (Deville et al. 2013). To calculate the gravity effect of water in the soil, we have constructed a model, which takes into account both topography and the umbrella effect caused by the laboratory building. The model is constructed from rectangular 3D blocks (voxels) with a horizontal size of 1 × 1 m and a vertical size of 0.1 m. The model extends over a horizontal area of 201 × 201 m and to 15 m in depth, and hence

Table 2

Studied rainfall cases 2014

Date	Tot	Event	Int	T020	N7	N6	GD	Dur	CN
14-06-12	24.5	24.1	12.2	7.08	4.73	4.95	− 2.35	1011	1
14-07-16	6.6	6.4	39.6	1.0	1.31	1.16	0.31	49	2
14-08-07	5.5	5.0	64.8	0.03	0.63	0.34	0.60	6	3
14-08-13	35.5	9.0	72.0	2.92	2.62	2.61	− 0.30	15	4
14-08-13	35.5	8.6	100.8	2.61	2.73	2.59	0.12	17	5
14-08-14	5	4.2	11.7	2.02	2.37	2.58	0.35	97	6
14-08-16	16.9	8.8	35.6	1.42	1.21	1.39	− 0.21	40	7
14-08-16	16.9	6.4	64.8	1.34	0.99	0.88	− 0.35	13	8
14-08-18	19.6	4.0	57.6	0.13	0.46	0.32	0.33	9	9
14-08-19	26.2	8.9	79.2	1.37	1.35	1.13	− 0.02	30	10
14-08-20	53	28.1	126	1.99	13.74	13.92	11.75	48	11
14-09-22	13.6	13.1	6.0	2.74	1.97	2.16	0.77	526	12
14-10-19	12.4	11.4	11.9	4.45	6.07	6.09	1.62	628	13
14-11-02	6.2	2.8	6.0	1.32	1.13	0.96	− 0.19	47	14
14-11-06	13.5	14.3	6.0	7.32	7.54	7.77	0.22	944	15

Precipitation data are recorded every second, but for analyses decimated to 1 min. The mean square difference between N6 and N7 sensors computed from 15 cases was 0.21 nms^{-2}

Date event day, *Tot* total amount of precipitation per day (mm), *Event* precipitation of event (mm), *Int* maximum intensity of rain (mmh^{-1}), *T020*, *N7*, *N6* gravity effect of events (nm/s^{-2}), *GD* gravity difference (N7-N6) (nms-2), *Duration* event duration (min), *CN* case number

comprising a total of 6,060,150 voxels. The horizontal extension of the model is shown in Fig. 1. We calculated the gravity effect at the sensor position exactly for each rectangular voxel, using different densities (Nagy 1966). We used 2600 kg m^{-3} for bedrock and 1400 kg m^{-3} for soil. We did not consider the voxels directly below the gravity laboratory. The soil depth was determined by gravimetric methods (Elo 2001, 2006). Gravity measurements were carried out in a grid with a distance of about 5 m (within 50 m from the gravity laboratory) and 10 m further away. Topographic heights were determined using RTK GPS. Maximum thickness was 3.7 m and the mean was 0.8 m.

Water in the soil was simulated using higher densities for the respective voxels. We exploited rain gauges, soil-moisture sensors, the tubes measuring the water level in the sediments and weather data for estimating temporary water content in the soil. In addition, we can add to the model snow with variate densities above soil. In Fig. 11 we present the topography of the area shown in Fig. 1. Height profiles for surface and bedrock along the dotted lines shown in Fig. 1 are presented in Fig. 12. In Table 3 we provide results of some model calculations, for different soil water content, using two sensor locations separated by 3 m in WE direction (Fig. 1) representing T020 and N7, respectively. First we have calculated the gravity effects without extra water. Then we have added 100 mm water in the top of the soil layer, then 100 mm water on top of the bedrock and finally fully saturated soil. The total recorded precipitation for the study period was 990 mm. From Table 3 we can see that as a part of bedrock rises above of N6/N7, it causes a negative effect. Moderate added extra mass did not increase the difference between the two sensor sites. Only a large amount of extra mass produced an increasing difference. We have looked into other possibilities for "hidden" water.

Effects of the fracture water of bedrock on superconducting gravimeter data were studied by Hokkanen et al. (2007) using a ground penetration Radar (GPR) around the laboratory (22 × 22 m). Maximum effect could be several nms^{-2}. However, we do not have information of water exchange and fractures below the gravity laboratory.

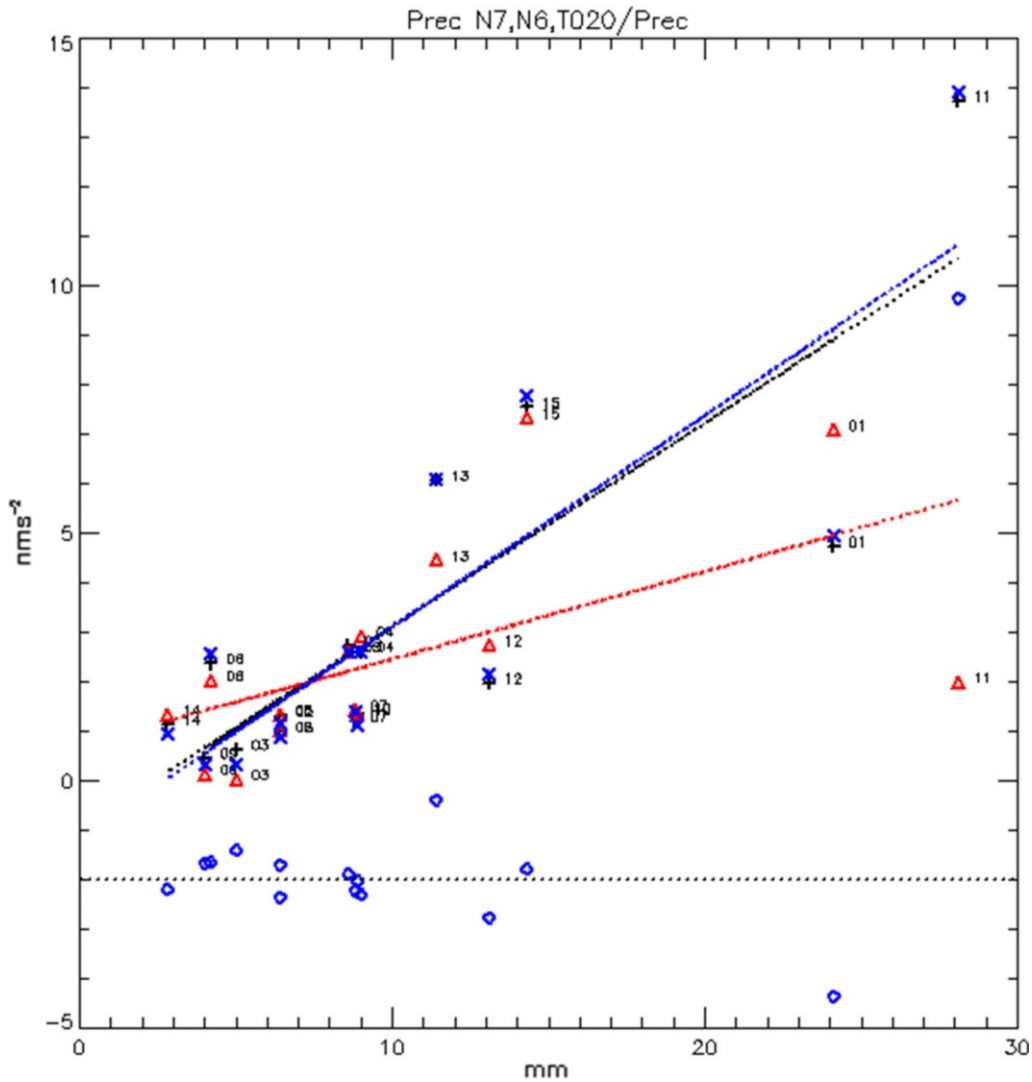

Figure 10
Observed gravity effect (nms^{-2}) due to rain events (mm) presented in Table 2. N7 shown with black + sign, N6 with blue *x* and T020 with red triangles. Dotted lines are regressions between gravity and amount of rain. Difference between sensors N7-T020 is presented by blue diamonds. Regression coefficient for N7 is 0.41 nms^{-2} mm^{-1} (± 0.08), for N6 it is 0.43 nms^{-2} mm^{-1} (± 0.08) and for T020 0.18 nms^{-2} mm^{-1} (± 0.07)

4. Conclusions

The difference in annual variations between the two OSG-073 and T020 gravimeters is remarkable and reaches up to 20 nms^{-2}. By comparing two sensors separated by only 3 m, we have illustrated a horizontal gravitational effect due to local hydrology at Metsahovi station. The difference in the gravity signal is biggest in July–August, when the soil is dry. Abundant precipitation in August and September reduce the difference. T020 is on the middle of a bedrock hill and N7 was situated closer to the soil. Model calculations show that 100 mm of water on soil areas of ME produces a gravity effect of 8 nms^{-2} (Mäkinen et al. 2014) (Table 3). It could mean that evaporation or runoff of about 250 mm water from the soil around the gravity laboratory corresponds to about 20 nms^{-2} in gravity. Annual variations in

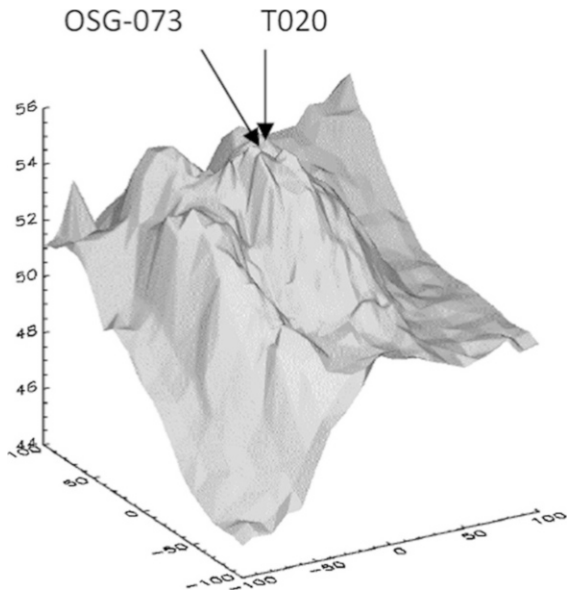

Figure 11
The map in Fig. 1 presented as shaded surfaces with position of gravimeters. Dimensions are in m

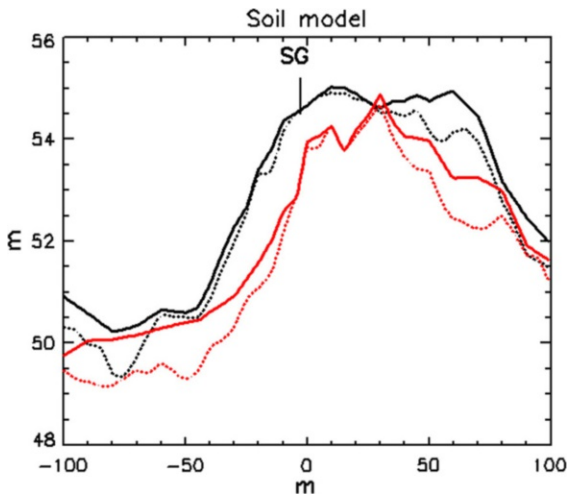

Figure 12
Height profiles presented in Fig. 1. Profile passing SG (T020) is shown in black and profile 20 m to west in red. Solid lines mean height of terrain and dotted lines are height of bedrock. The soil including water is modeled between these layers.

groundwater in bedrock and water in fractures have a lesser effect on T020. Uneven snow cover can cause gravity effects up to 20 nms^{-2}, especially if snow is on the roof of the laboratory (Virtanen 2000). During the winter 2014–2015, snow cover was smaller than usual and there were no significant amount of snow on the laboratory roof. During rainfall, the gravity difference between the SG sensors seems (Table 2) to have a weak connection with the duration of the rain event (Table 2, cases 1 and 11). Rain events 1 and 11 (Table 2) have about the same amount of rain but different duration. In the special case 11, lot of water was quickly accumulated near the sensors N6 and N7. Water accumulation was probably due to the location of downspout, which leads the water from the roof to a pass between gravity laboratory and main building.

Annual precipitation can be 800 mm, thus moderate precipitation (100 mm) in our model cannot give observable gravity differences between different sensor locations. It is evident that we will need more detailed model near the sensors and observations from instantaneous runoff areas.

To get more information, we will continue parallel observation with two SGs, one is iOSG-022 (N6) at the same place as OSG-073 and iGrav-013 (N7) located on the same pier as T020 before.

Table 3

Gravity response (nms^{-2}) of different gravimeters to water added to the model

Water	N6/N7	T020	Difference
No add water	− 6.9	0.0	− 6.9
Soil upper 100	+ 1.6	+ 8.5	− 6.9
Soil lower 100	+ 3.1	+ 10.1	− 7.0
Soil whole 100	+ 43.1	+ 53.1	− 10.0

Soil upper (100) means 100 mm water in upper part of soil; soil lower means 100 mm water above bedrock. Soil 100 means 100 mm water in the whole soil layer

Acknowledgements

Special thanks to Richard Warburton and Jyri Näränen for installation work of OSG-073.

References

Deville, S., Jacob, T., Chéry, J., & Champollion, C. (2013). On the impact of topography and building mask on time varying gravity due to local hydrology. *Geophysical Journal International, 192,* 82–93.

Elo, S. (2001) Irtomaan paksuuden arviointi painovoimamittausten avulla (Working report in Finnish). Geological survey of Finland

Elo, S. (2006) 3D modelling of overburden thickness at Metsähovi. Abstract. Geological survey of Finland

Goodkind, J. M. (1999). The superconducting gravimeter. *Review of Scientific Instruments, 70*(11), 4131–4152.

Hinderer, Crossley, Warburton (2007) Treatise on geophysics, Vol 3, Superconducting Gravimetry, Elsevier.

Hokkanen, T., Korhonen, K., & Virtanen, H. (2006). Hydrogeological effects on superconducting gravimeter measurements at Metsähovi, Finland. *Journal of Environmental and Engineering Geophysics, 11*(4), 261–267.

Hokkanen, T., Korhonen, K., Virtanen, H., & Laine, E.-L. (2007). Effects of the fracture water of bedrock on superconducting gravimeter data. *Near Surface Geophysics, 5*(2), 133–139. **(82007)**.

Mäkinen, J., Hokkanen, T., Virtanen, H., Raja-Halli, A., Mäkinen R.P. (2014) Local hydrological effects on gravity at Metsähovi, Finland: implications for comparing observations by the superconducting gravimeter with global hydrological models and with GRACE. In: Proceedings of the International Symposium on Gravity, Geoid and Height Systems GGHS 2012, October 9–12, 2012, Venice, IAG Symposia 141

Meurers, B. (2007). Correcting superconducting gravity time-series using rainfall modeling at the Vienna and Membach stations and application to Earth tide analysis. *Journal of Geodesy, 81,* 703–712. https://doi.org/10.1007/s00190-007-0137-1.

Nagy, D. (1966). The gravitational attraction of right rectangular prism. *Geophysics, 31,* 361–371.

Peterson, J. (1993) Observations and modelling of seismic background noise, US Geol. Surv. Open-File Rept. 93–332, Albuquerque, New Mexico

Rosat, S., & Hinderer, J. (2011). Noise levels of superconducting gravimeters: updated comparison and time stability. *Bulletin of the Seismological Society of America, 101*(3), 1233–1241.

Rosat, S., Hinderer, J., Boy, J.P., Littel, F., Boyer, D., Bernard, J.D., Rogister, Y., Mémin, A., Gaffet, S. (2016). First analyses of the iOSG-type superconducting gravimeter at the low noise underground laboratory (LSBB URL) of Rustrel, France, E3S Web of Conf., 12, 06003. doi:https://doi.org/10.1051/e3sconf/20161206003

Van Camp, M., & Vauterin, P. (2005). Tsoft: graphical and interactive software for the analysis of time series and Earth tides. *Computers and Geosciences, 31*(5), 631–640. https://doi.org/10.1016/j.cageo.2004.11.015.

Vehviläinen, B. (2007). Hydrological forecasting and real-time monitoring: the watershed simulation and forecasting system (WSFS). https://doi.org/10.1002/9780470511121.ch2.

Virtanen, H. (2006). Studies of earth dynamics with the superconducting gravimeter, academic dissertation in geophysics, Helsinki. Also published as No. 133 in the series of: publications of the Finnish Geodetic Institute. http://hdl.handle.net/10138/23166. Accessed 14 Nov 2017.

Virtanen, H., Bilker-Koivula, M., Mäkinen, J., Näränen, J., & Ruotsalainen, H. (2014). Comparison between measurements with the superconducting gravimeter T020 and the absolute gravimeter FG5-221 at Metsähovi, Finland in 2003–2012. *Bulletin d'Information des Marées Terrestres, 148,* 11923–11928.

Virtanen, H., & Kääriäinen, J. (1995). The installation of and first results from the superconducting gravimeter GWR20 at the Metsähovi station. *Reports of the Finnish Geodetic Institute, 95,* 1.

Virtanen, H., & Kääriäinen, J. (1997). The GWR T020 Superconducting gravimeter 1994–1996 at the Metsähovi station, Finland. *Reports of the Finnish Geodetic Institute, 97,* 4.

Voigt, C., Förste, C., Wziontek, H., Crossley, D., Meurers, B., Pálinkáš, V., et al. (2016). *Report on the data base of the international geodynamics and earth tide service (IGETS), (scientific technical report STR—Data; 16/08)*. Potsdam: GFZ German Re-search Centre for Geosciences. https://doi.org/10.2312/GFZ.b103-16087.

(Received December 16, 2016, revised November 1, 2017, accepted November 5, 2017, Published online November 17, 2017)